Taylor & Francis
Taylor & Francis Group

Research Article

A comparative analysis of DEM-based models to estimate the solar radiation in mountainous terrain

J. A. RUIZ-ARIAS, J. TOVAR-PESCADOR*, D. POZO-VÁZQUEZ and
H. ALSAMAMRA

Atmospheric Modelling and Solar Radiation Group, Department of Physics, Campus
Las Lagunillas, University of Jaén, 23071 Jaén, Spain

Daily solar radiation estimates of four up-to-date solar radiation models (*Solar Analyst*, *r.sun*, *SRAD* and *Solei-32*), based on a digital elevation model (DEM), have been evaluated and compared in a Mediterranean environment characterized by a complex topography. The models' estimates were evaluated against 40 days of radiometric data collected in 14 stations. Analyzed sky conditions ranged from completely overcast conditions to clear skies. Additionally, the role of the spatial resolution of the DEM has been evaluated through the use of two different resolutions: 20 and 100 m. Results showed that, under clear-sky conditions, the daily solar radiation variability in the study area may be reasonably estimated with mean bias errors under 10% and root mean square error values of around 15%. On the other hand, results proved that the reliability of the estimates substantially decreases under overcast conditions for some of the solar radiation models. Regarding the role of the DEM spatial resolution, results suggested that the reliability of the estimates for complex topography areas under clear-sky conditions improves using a higher spatial resolution.

Keywords: Solar radiation model; Digital elevation model; GIS; Irradiance; Complex topography

List of symbols

z	Elevation above sea level
Z	Zenith angle
α	Solar height angle
β	Surface slope angle
θ	Incidence angle of the solar beam
Ψ	Azimuth angle
ε	Eccentricity of the Earth's orbit
I_s	Solar constant
I_{0n}	Extraterrestrial normal irradiance
I_{0h}	Extraterrestrial horizontal irradiance
I_{Gn}	Global normal irradiance
I_{Bn}	Beam normal irradiance
I_{Bnc}	Clear sky normal beam irradiance
I_{Bh}	Beam horizontal irradiance

*Corresponding author. Email: jtovar@ujaen.es

I_{Dh}	Diffuse horizontal irradiance
I_{Bi}	Beam irradiance on a tilted surface
I_{Di}	Diffuse irradiance on a tilted surface
I_R	Reflected irradiance
T_L	Turbidity coefficient of Linke (monthly averaged parameter)
δ_R	Rayleigh optical thickness
m	Relative optical air mass
τ	Transmittance of the atmosphere
τ_z	Atmospheric transmittance at elevation z above sea level
τ_{sl}	Atmospheric transmittance at sea level
k_t	Hourly clearness index of the solar radiation
k_d	Hourly diffuse fraction of the solar radiation
G_h	Daily global irradiation
K_c	Clear-sky index
G_{hc}	Daily global irradiation under clear sky conditions
v	Sky-view factor
CIRC	Circumsolar correction factor
ALB	Ground albedo
Q_S	Monthly averaged irradiation
Q_0	Clear sky monthly averaged irradiation
SF	Monthly averaged sunshine fraction
ξ	Cloudiness parameter

Special notation for *Solar Analyst*:

$I_B^{Z,\Psi}$	Direct radiation from the sun-map sector with zenith Z and azimuth Ψ
$ST^{Z,\Psi}$	Time duration represented by the sky-map sector with zenith Z and azimuth Ψ
$SG^{Z,\Psi}$	Non obstructed gap fraction for the sun-map sector with zenith Z and azimuth Ψ
$\theta^{Z,\Psi}$	Incidence angle between the sky-map sector with zenith Z and azimuth Ψ and the axis normal to the terrain surface
$I_D^{Z,\Psi}$	Diffuse radiation from the sky-map sector with zenith Z and azimuth Ψ
P_D	Proportion of global normal radiation flux that is diffuse
T	Time interval for analysis of the diffuse radiation
$SKG^{Z,\Psi}$	Gap fraction (proportion of visible sky) for the sky-map sector with zenith Z and azimuth Ψ
$W^{Z,\Psi}$	Proportion of diffuse radiation originating in a given sky-map sector relative to all sectors
Z_1, Z_2	Bounding zenith angles of the of the sky-map sector
N_Ψ	Number of azimuthal divisions in the sky-map

1. Introduction

The solar radiation is a major forcing function of physical and biologic processes on our planet (Dubayah and Rich 1995). The spatial and temporal heterogeneity of incoming solar radiation determines the dynamic of the agricultural (Reuter *et al.* 2005), ecologic (Kumar and Skidmore 2000) or hydrologic (McVicar *et al.*, 2007) processes. Therefore, knowledge of the spatial variability of radiation components is crucial in order to understand these processes. Additionally, this knowledge is a key tool in supporting policies of renewable and efficient energies.

Many factors and processes interact to determine the amount of solar radiation received at a given point on the Earth's surface. Particularly, if a detailed understanding of the incoming solar radiation at local scale is attempted, factors such as surrounding topography, albedo and forest canopy should be taken into account (McKenney *et al.* 1999; Corripio 2003; López *et al.* 2007). Furthermore,

topography changes the proportion of direct and diffuse radiation in the solar global radiation through the shadow-casting effect, for example. Therefore, diffuse and reflected components of the radiation become more important when the topography increases its complexity (Kondratyev 1965).

Variability in elevation, surface orientation (slope and aspect) and shadow cast by topographic features create strong local gradients of insolation. Different interpolation techniques have been proposed to derive spatial databases from measurements of meteorologic and climatology stations, such as spline functions (Sampson and Guttorp 1992; Xia *et al.* 2000; Jeffrey *et al.* 2001) or weighted average procedures and kriging (Zelenka *et al.* 1992; Hulme *et al.* 1995). Such techniques provide reasonable estimates in flat terrain with homogeneous climatologic properties, but reliability decreases when the complexity of the topography increases (Tovar *et al.* 1995). Furthermore, in some cases, these techniques become infeasible because of the high topographic heterogeneity. Additionally, interpolation techniques need a considerable amount of insolation monitoring stations that are seldom available. Interpolation appears to be a useful method for a station density of about $1000 \, km^2$/station, but the quality of interpolated data in complex topographies quickly drops with height, mainly because of the potential snow cover and cloud distribution effects on the incoming radiation (Scheifinger and Kromp-Kolb 2000). This is a great limitation, given that the largest station densities are localized in the proximities of urban areas which usually have a homogeneous terrain, and they usually decrease as the complexity of the terrain increases.

Spatially continuous irradiance values can also be derived directly from meteorologic geostationary satellites. But satellite data provide less accurate values compared to ground measurements, particularly under overcast sky conditions. In contrast to the high cost of building and maintaining insolation monitoring stations, and the relatively coarse spatio-temporal resolution of the satellite estimates, spatially-based solar radiation models provide a cost efficient way of characterizing the spatial and temporal variability of insolation. Several models have been developed in the last decade such as *SolarFlux* (Hetrick *et al.* 1993; Dubayah and Rich 1995), *Solei-32* (Miklánek and Mészáros 1993; Mészáros and Miklánek 2002), *Solar Analyst* (Fu and Rich 2000), *SRAD* (Wilson and Gallant 2000) and *r.sun* (Hofierka and Súri 2002). They have shown their usefulness and reliability in fields as hydrology (O'Loughlin 1990; McVicar *et al.* 2007), environmental sciences and land management (Kumar *et al.* 1997; McKenney *et al.* 1999; Kumar and Skidmore 2000; Fu and Rich 2002; Oliphant *et al.* 2003; Reuter *et al.* 2005), renewable energies (Súri and Hofierka 2004; Súri *et al.* 2005) or climatology (Tovar-Pescador *et al.* 2006; Batlles *et al.* 2008).

These models use the topographic information contained in a digital elevation model (DEM) to determine topographic features such as elevation, surface orientation and shadow casting and based on this information, to estimate the incoming solar radiation at every point of the DEM. However, these models follow very different approaches to obtain these estimates. Additionally, it should be noted that the same DEM with different resolutions will usually produce different estimations of elevation, slope, aspect (Raaflaub and Collins 2006) and shadowing, especially in complex topographies. Consequently, they may provide different estimations of solar radiation. Finally, the increase in the resolution of the DEM causes a squared increase in the computational cost of the process.

In this work, we evaluate and compare daily solar radiation estimates provided by four up-to-date spatially-distributed solar radiation models: *Solar Analyst*, *r.sun*, *SRAD* and *Solei-32*, in a Mediterranean environment. Particularly, the study has been carried out for a region located within the National Park of Sierra Nevada (South-Eastern Spain). This area, characterized by a complex topography, represents a typical middle-high mountainous landscape on the Mediterranean basin. Models estimates were tested against 40 days of radiometric data, collected in fourteen stations located in this region. The location of the stations represents a wide range of topographic conditions. The radiometric data were selected in order to cover all kind of sky conditions, based on the daily clearness index, (ratio of daily global horizontal irradiation at ground level to the daily extraterrestrial horizontal solar irradiation), and different climatic conditions along the year. Additionally, the role of the DEM resolution in the daily solar radiation estimates of the solar radiation models is also evaluated through the use of DEMs with two different spatial resolutions: 20 and 100 m.

The work is organized as follows. Section 2 deals with the general features and the specific methods implemented in the solar radiation models. The third section describes the study region and the experimental data used to test the results. Section 4 describes, for each of the models, the methodology employed to obtain the solar radiation estimates. Finally, the results are presented and some conclusions highlighted in, respectively, Sections 5 and 6.

2.   General description of the solar radiation models

Spatial solar radiation models provide a cost-efficient means for understanding the spatial and temporal variation of insolation over landscape scales (Dubayah and Rich 1995, 1996; Tovar-Pescador *et al.* 2006). For mountain terrains, such models are best made available within a Geographical Information System (GIS) platform as *ArcGIS*, *IDRISI* or *GRASS*. These GIS environments make it easier to account for shadow-casting and reflections and allow relating the solar radiation estimates with other parameters as land cover.

The four solar radiation models considered in this work follow three different approaches in the assessment of the daily solar irradiation. *Solar Analyst* implements a geometrical approach that splits the sky into different sectors defined by their zenith and azimuth coordinates. The atmospheric attenuation is taken into account by means of the direct atmospheric transmittivity and the proportion of diffuse radiation. *SRAD* uses a series of monthly averaged parameters (as atmospheric transmittivity or sunshine fraction, among others) to adjust the estimates previously obtained. The *r.sun* and *Solei-32* models account for the atmospheric attenuation for clear-skies through the turbidity coefficient of Linke, so they need a subsequent correction using ground measurements to consider the cloud effects. In the next sections, a more detailed description of the procedures used by the four models to compute the solar radiation is presented.

2.1   *Solar Analyst*

Solar Analyst is an ArcView v3.x extension that runs on a Windows environment. It can calculate insolation considering site latitude, topography, shadow cast and atmospheric attenuation. It yields global, direct and diffuse irradiation as well as direct irradiation duration, sunmap, skymap and viewshed.

As the first step during its operation, *Solar Analyst* generates an upward-looking hemispherical viewshed (a virtual fisheye photography) for every location on the DEM. The amount of direct solar radiation originated from each sky direction is represented by creating a sunmap in the same hemispherical projection as for the viewshed. It maps the apparent position of the sun by discrete sky sectors as it varies through the time. Total direct insolation is the sum of the direct insolation from all sunmap sectors unobstructed (or partially unobstructed) by the viewshed. The direct insolation from a sunmap sector ($I_B^{Z,\Psi}$) with centroid at zenith angle Z and azimuth angle Ψ is then calculated using the following equation

$$I_B^{Z,\Psi} = I_s \tau^m ST^{Z,\Psi} SG^{Z,\Psi} \cos \theta^{Z,\Psi} \tag{1}$$

where I_S is the solar constant, τ is the direct transmittivity of the atmosphere, m is the relative optical path length, $ST^{Z,\Psi}$ is the time duration represented by the sky sector, $SG^{Z,\Psi}$ is the non obstructed gap fraction for the sunmap sector and $\theta^{Z,\Psi}$ is the angle of incidence between the centroid of the sky sector and the axis normal to the surface (Fu and Rich 2000).

Unlike direct radiation, diffuse solar radiation can be originated from any sky direction. *Solar Analyst* divides the whole sky into a series of sky sectors defined by zenith and azimuth coordinates. Each sector is assigned a unique value according to the sky scheme selected. This is a raster map known as skymap. Total diffuse insolation is the sum of the diffuse insolation from all skymap sectors unobstructed (or partially unobstructed) by the viewshed. For each sky sector, the diffuse radiation at its centroid ($I_D^{Z,\Psi}$) is calculated, integrated over the time interval (T) and corrected by the gap fraction ($SKG^{Z,\Psi}$) and angle of incidence ($\theta^{Z,\Psi}$), using the following equation

$$I_D^{Z,\Psi} = I_{Gn} P_D T SKG^{Z,\Psi} W^{Z,\Psi} \cos \theta^{Z,\Psi} \tag{2}$$

where I_{Gn} is the global normal radiation calculated by summing the direct radiation from every sector (including obstructed sectors) without correction for angle of incidence, and then correcting for the proportion of direct radiation, which equals to $1-P_D$, where P_D is the proportion of global normal radiation flux that is diffuse. $W^{Z,\Psi}$ is the proportion of diffuse radiation originating in a given sky sector relative to all sectors which, for the uniform sky diffuse model used in these simulations, is calculated as

$$W^{Z,\Psi} = (\cos Z_1 - \cos Z_2)/N_\Psi \tag{3}$$

being Z_1 and Z_2 are the bounding zenith angles of the sky sector and N_Ψ is the number of azimuthal divisions in the skymap (Fu and Rich 2000).

Global irradiation is calculated as the sum of direct and diffuse irradiation of all sectors. All these calculations are repeated for every location on the topographic surface, thus producing insolation maps for an entire geographic area.

2.2   *r.sun*

The *r.sun* is based on Hofierka (1997) and developed under the GRASS GIS open source environment (http://grass.osgeo.org). The first version of *r.sun* was significantly re-engineered by Súri and Hofierka (2004) by implementing algorithms developed within the European Solar Radiation Atlas (ESRA) (Beyer *et al.* 1997; Page *et al.* 2001). It provides the three components of solar radiation (direct, diffuse

and reflected) for clear sky conditions. In case of overcast conditions, a cloud attenuation factor must be used. The model also considers the spatial variation of solar radiation due to terrain and terrain-shadowing effects (Hofierka and Súri 2002). Its applicability has also been shown for large regions, as the European continent, in the PVGIS project (http://re.jrc.ec.europa.eu/pvgis/index.htm) using a DEM with a resolution of $1\,km^2$.

For a clear-sky atmosphere, *r.sun* describes the attenuation by the gas constituents based on its relative optical air mass (m) and the Rayleigh optical thickness (δ_R). The attenuation by solid and liquid particles is described by the Linke's turbidity (T_L), which changes with geographical location, time and elevation. Overcast conditions cause the strongest attenuations on the solar global irradiation and *r.sun* does not provide any input parameter to consider these situations, so an empirical approach has to be used.

The clear-sky normal beam irradiance normal to the solar beam I_{Bnc} is calculated as

$$I_{Bnc} = I_{0n}e^{-0.8662T_L m\delta_R} \tag{4}$$

where I_{0n} is the extraterrestrial irradiance normal to the solar beam corrected for the Earth's eccentricity. The relative optical air mass (m) depends on the declination, the latitude and the solar hour angle. Furthermore, it is corrected for elevation. The Rayleigh optical thickness (δ_R) depends exclusively on the relative optical air mass (Hofierka and Súri 2002). Once I_{Bnc} is calculated, it is projected on the inclined surface according to its slope and aspect.

The estimate of the diffuse component on a horizontal surface I_{Dh} is made as the product of the normal extraterrestrial irradiance I_{0n}, a diffuse transmission function T_n (dependent only on the Linke turbidity factor), and a diffuse solar altitude function F_d (dependent only on the solar altitude α)

$$I_{Dh} = I_{0n}T_n(T_L)F(\alpha) \tag{5}$$

The model for estimating the clear-sky diffuse irradiance on an inclined surface distinguishes between sunlit, potentially sunlit and shadowed surfaces and is calculated from the diffuse component on a horizontal surface I_{Dh} (Hofierka and Súri 2002).

The ground reflected clear-sky irradiance relies on an isotropic assumption and is proportional to the global horizontal irradiance (given as the sum of the direct and diffuse components), to the mean ground albedo and to the fraction of the ground viewed by an inclined surface (Hofierka and Súri 2002).

2.3 *SRAD*

This model is freely distributed by the USC *GIS Research Laboratory* (http://www.uscgislab.net) as part of the TAPES-G (*Terrain Analysis Programs for the Environmental Sciences*) program. It is available under a UNIX environment although the latest versions were also designed to run inside the ArcGIS9.x geo-processing framework on Windows platforms and this is the version used in this study. It provides the complete radiation budget through the short- and long-wave components, the net irradiance as well as the surface and air temperatures.

The model calculates potential solar radiation (both short-wave and long-wave radiation) as a function of latitude, slope, aspect, topographic shading and time of year and then modifies this estimate using information about monthly average cloudiness and sunshine hours. The short- and long-wave radiation fluxes are then used to estimate the surface energy budget at every grid point for a user-specified period, ranging from 1 day to 1 year (Wilson and Gallant 2000).

Calculation of short-wave radiation in *SRAD* is divided into four steps. First, the horizontal extraterrestrial irradiance is computed. The different clear-sky instantaneous short-wave fluxes are obtained in the next step for every cell of the DEM at 12 minutes intervals symmetrically around noon, from sunrise to sunset. This treatment relies on the work of Fleming (1987), who concluded that this approach yields sufficiently accurate daily estimates for most of the hydrologic, geomorphologic and ecologic applications for what *SRAD* was conceived. In the third step, these fluxes are integrated to obtain daily totals and adjusted to account for the effects of the cloudiness. Finally, the fourth step implies to average daily values over the period specified by the user.

To compute the direct and diffuse horizontal fluxes for clear-sky conditions, *SRAD* provides two approaches: a lumped transmittance and an individual transmittance of the components. The first approach is now briefly depicted because it was chosen in this study for similarity with the other solar radiation models evaluated in this work. In this approach, the horizontal direct solar beam flux is calculated as

$$I_{Bh} = I_{0h}\varepsilon\tau^{m} \tag{6}$$

where I_{Bh} is the horizontal extraterrestrial irradiance corrected for the Earth's eccentricity (ε), τ is the transmission coefficient or fraction of radiation incident at the top of the atmosphere which reaches the ground along the vertical path, and m is the relative optical mass calculated as $m = \sec(Z)$. The transmission coefficient is corrected according the grid cell elevation as

$$\tau = \tau_{sl} + t_{lapse}z \tag{7}$$

where τ_{sl} is the transmission coefficient at sea level, t_{lapse} typically equals $0.00008\,\mathrm{m}^{-1}$ and z is the elevation above sea level (Wilson and Gallant 2000).

The instantaneous diffuse irradiance is estimated as

$$I_{Dh} = (0.271 - 0.294\tau^{m})I_{0h}\varepsilon \tag{8}$$

showing that the transmittance of scattered skylight decreases as the direct solar beam transmittance increases (Wilson and Gallant 2000).

A correction is applied to consider as direct beam the diffuse radiation from within $5°$ of the direct solar beam. This is taken into account by the circumsolar coefficient (CIRC) defined as the fraction of diffuse radiation derived from within $5°$ of the direct solar beam (Wilson and Gallant 2002)

$$I_{Dh} = I_{Dh} - I_{Dh}\text{CIRC} \tag{9}$$

$$I_{Bh} = I_{Bh} - I_{Dh}\text{CIRC} \tag{10}$$

The direct irradiance on a tilted surface I_{Bi} can be calculated based on I_{Bh} (previously corrected for the circumsolar fraction) and the angle θ subtended between the solar beam and the normal to the surface. The isotropic diffuse radiation is calculated just as $I_{Di}=I_{Dh}v$, where v is the sky-view factor and the reflected radiation is estimated as $I_R=(I_{Bh}+I_{Dh})(1-v)ALB$, where ALB is the ground albedo (Wilson and Gallant 2002).

The effect of overcast skies is taken into account by means of the sunshine fraction (defined as the observed duration of sunshine out of the maximum possible) and the cloudiness transmittance (defined as the fraction of radiation received when the sky is overcast).

2.4 *Solei-32*

This model was developed in the *Institute of Hydrology of Slovak Academy of Science* (http://www.ih.savba.sk) by Miklánek and Mészáros (1993) for a DOS environment. It optionally requires land cover, ground albedo and meteorologic data. This last data consists of a file with values of relative sunshine, temperature, wind, relative air humidity and vapor pressure for all the control sites defined in the study area. If only land cover and/or ground albedo data are provided, *Solei-32* will yield the potential incoming solar radiation. The model, first, computes the topographic attributes and sunshine duration at every time step for every cell on the DEM. Then, the estimation of potential energy incoming on the inclined surface is carried out as the sum of direct, diffuse and reflected components. For those cell grids where direct sunshine duration is equal to zero, the potential energy income is assumed to be equal only to diffuse radiation.

The normal direct flux I_{Bn} is calculated as

$$I_{Bn} = I_{0n} \frac{\sin\alpha - 0.1\,TL(T_L-1)/30}{\sin\alpha + 0.106\,T_L} \tag{11}$$

where I_{0n} is the normal extraterrestrial irradiance. The inclined direct radiation is obtained projecting I_{Bn} on the inclined surface as: $I_{Bi}=I_{Bn}\cos(\theta)$ (Mészáros and Miklánek 2002).

The diffuse component assessment for the inclined surface is carried out according to

$$I_{Di} = \frac{1}{2} I_{Dh} \left[1 + \cos\beta + \sin\beta \left(0.94 e^{\cos\theta} + \frac{1.84}{T_L} - 1.44 \right) \right] \tag{12}$$

and

$$I_{Dh} = (0.220 + 0.025 T_L)(I_{0n} - I_{Bn})\sin\alpha \tag{13}$$

where β is the surface slope (Mészáros and Miklánek 2002).

The reflected radiation is estimated as

$$I_{Ri} = 0.5\,ALB(1 - \cos\beta)(I_{Dh} + I_{Bn}\sin\alpha) \tag{14}$$

3. Experimental data

The study area is located within the National Park of Sierra Nevada (South-Eastern Spain), the largest National Park of Spain (Figure 1). It presents a very complex
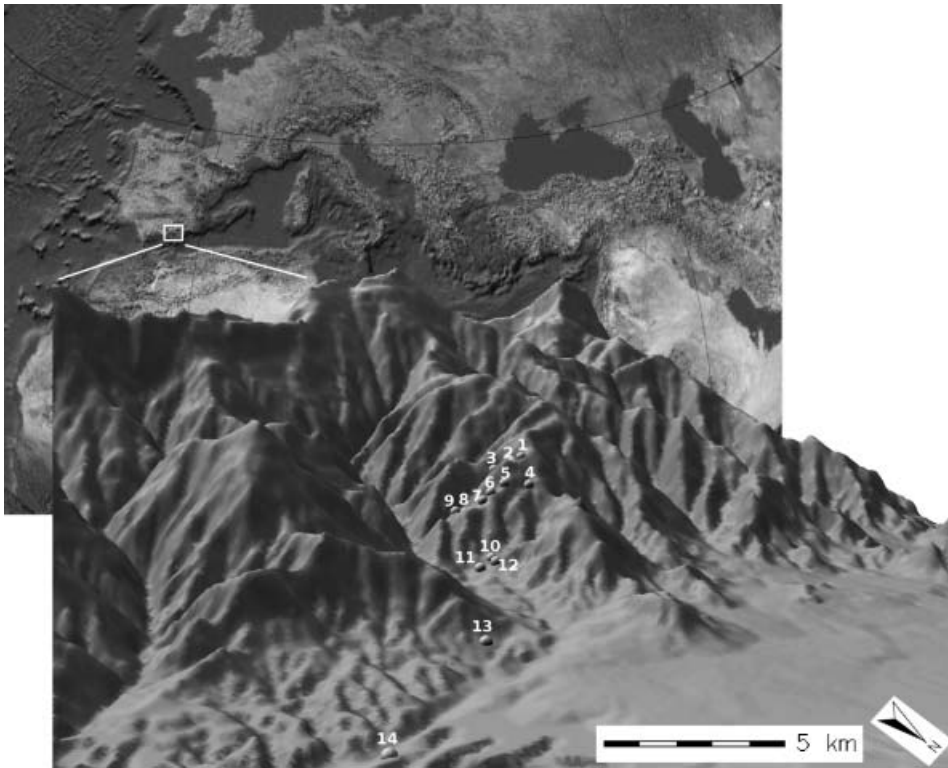
Figure 1. Study area and location of the 14 radiometric stations within the National Park of Sierra Nevada.

topography with elevations ranging from 500 to 3482 m (Mulhacen peak). The climate is that of a typical middle and high Mediterranean mountainous environment, with dry hot summers, cold winters and relatively high precipitation during autumn and spring.

Fourteen meteorologic stations were located in the northern side of the Sierra Nevada Park, in an area of $10 \times 5 \, km^2$. This area can be classified into two sub-regions: the first one presents an almost flat area, containing two of the stations, and the other one, with the remaining stations, shows a complex topography. To sum up, the locations of the stations cover a wide range of elevations, aspects and slopes summarized in Table 1.

HOBO (*Onset Corporation*) data-loggers were employed to collect temperature (Onset TMC6-HB probe) and global radiation data (Licor 200-SZ radiometer) on horizontal and inclined surfaces. An annual calibration and inter-comparison of the sensors is carried out. The estimated instrumental error is less than 5%, typically 3%. All data were recorded on a 2.5 minutes basis.

In the present study, we use data corresponding to the period from March 2003 to January 2006. Forty days have been chosen along this period trying to homogeneously cover all the sky conditions and all the months of a natural year. The sky conditions were analyzed based on the clearness index which, in this set of data, ranges from 0.1 to 0.77. Along the year, there are 13 days from January to April, 14 days from May to August and 13 days from September to December. On average, there are 3 days per month, which ensures a proper sample of the different

Table 1. Topographic features of the 14 radiometric stations used in this work. Both measured and DEM estimated values with 20 and 100 m of spatial resolution, are displayed.

	Elevation (m.a.s.l.)			Slope (°)			Aspect (°)		
Station	Measured	20 m DEM	100 m DEM	Measured	20 m DEM	100 m DEM	Measured	20 m DEM	100 m DEM
1	1659	1670	1637	10	24.7	15.8	45.0	150.6	122.0
2	1669	1647	1621	14	18.2	7.9	225.0	188.7	120.3
3	1619	1623	1580	13	18.2	16.8	202.5	171.3	131.6
4	1558	1562	1557	9	11.4	14.9	135.0	119.7	19.8
5	1565	1568	1555	5	11.4	12.7	180.0	82.9	54.9
6	1532	1537	1521	11	13.3	8.7	90.0	148.0	78.7
7	1505	1505	1492	3	12.8	10.6	180.0	83.7	82.3
8	1467	1460	1446	19	8.5	9.1	180.0	180.0	104.5
9	1449	1447	1471	19	26.7	9.4	202.5	84.3	105.7
10	1305	1301	1308	5	6.1	7.9	45.0	45.0	59.7
11	1292	1276	1282	15	3.2	5.5	157.5	63.4	51.3
12	1300	1299	1283	8	14.6	6.9	157.5	106.7	85.2
13	1188	1156	1172	0	7.1	6.0	0	0.0	19.3
14	1091	1077	1058	6	7.7	2.6	157.5	158.2	102.5

atmospheric conditions along the year. Additionally, the selected days represent a homogeneous range of sky conditions: the clearness-index is less than 0.3 for 10 days, between 0.3 and 0.6 for 20 days and greater than 0.6 for 10 days. To sum up, the criterion used for selecting the 40 days of evaluation, along with the range of topographic characteristics of locations of the 14 stations, ensures the coverage of a wide range of climatical and meteorologic conditions.

In order to study the influence of the DEM's resolution on the daily solar irradiation estimates of the solar radiation models, two models of 20 m (DEM20 hereinafter) and 100 m (DEM100 hereinafter) have been used and the results are compared with each other. Both DEM20 (782,825 grid cells) and DEM100 (31,668 grid cells) map exactly the same region, of about 300 km^2. The DEM20 were digitalized from a contour map of the study region and the DEM100 was generated by averaging the DEM20. This area is large enough to avoid the solar irradiation estimates being affected by border effects in the radiometric station locations. The mean elevation is practically the same for both models: 1490 m above sea level for DEM20 and 1486 m for DEM100. Nevertheless, the differences increase in the case of mean slope (12.66° for DEM20 and 9.35° for DEM100) and dominant aspect (10.64° for DEM20 and 14.77° for DEM100, where 0° means north direction and increases clockwise). It is worth clarifying that as the aspect is a circular variable, the mean value has no sense. Therefore, the dominant aspect has been calculated by decomposing the aspect vector in its rectangular components and then determining the mean value for each component. The dominant aspect is the direction corresponding to the vector defined by the mean rectangular components.

As earlier mentioned, some of the radiation models need some external information for the solar radiation estimates. In this work, the Linke turbidity factor used in *r.sun* and *Solei-32* has been obtained from the *Solar Database Services* (http://www.soda-is.com). This database has been developed in the framework of the project 'SoDa. *Integration and exploitation of networked Solar radiation Databases for environment monitoring*', supported by the *European Commission*, and its accuracy is reported to RMSE=0.7T_{LK} units. Particularly, monthly

averaged values corresponding to the station 2 location have been used as representatives of the whole study area. The mean absolute error of this assumption for all months is 2.13% and the maximum is 3.56% for April. Additionally, the sunshine fraction values used in *SRAD* were obtained from the *IIASA Climate Database* created at the *International Institute for Applied System Analysis* to represent current global climate (Leemans and Wolfgang 1991).

4. Methodology

Although all models obviously present, as pointed in section two, common input parameters (DEM, day of year, latitude or time step), there are certain differences in the way they calculate the solar irradiation. For instance, in the case of *Solar Analyst*, atmospheric conditions are essentially modeled by the direct atmospheric transmittance and the diffuse proportion, while *r.sun* and *Solei-32* use the Linke turbidity. *SRAD* applies a monthly average-based approach to adjust the final result. Therefore, a previous analysis is necessary to obtain the specific input parameters of each of the solar radiation models. Station 2 was selected as the control site representative of the entire study region and therefore, used to compute the input parameters. This station was selected because, according to the global irradiance time series for the testing days, it presents the lowest shadow-casting, a desirable feature for proper parameter estimation. Stations 13 and 14 could also have been selected, but were ruled out because they are located relatively far away from the rest of the stations (Figure 1). The time step used in all the models has been 30 minutes except for *SRAD*, which always uses a 12 minutes step.

In order to quantitatively assess the performance of the solar radiation models, the mean bias error (MBE) and the root mean square error (RMSE) have been calculated. The first one is a measured of the systematic error of the model. It evaluates the tendency of the model to under- or overestimate the measured values and is desired to be equal to zero. Its value is obtained as

$$\text{MBE} = \frac{1}{N} \sum (p_i - m_i) \tag{15}$$

where p_i is the ith predicted value and m_i is the ith measured value.

The RMSE estimates the level of scattering of the predicted values and is desired to be equal to zero. It has been calculated as

$$\text{RMSE} = \left[\frac{\sum (p_i - m_i)^2}{N} \right]^{1/2} \tag{16}$$

We also provide the correlation coefficient and the slope and intercept of the best fit line of the estimates to the measured values.

4.1 *Solar Analyst*

As it has been already mentioned, this model requires two input parameters to take into account the effects of the atmosphere on the solar radiation. One of them is the transmittivity of the atmosphere (averaged over all wavelengths), defined as the proportion of exoatmospheric radiation transmitted as direct radiation at sea level along the shortest atmospheric path (i.e. from the direction of the zenith) (Fu and

Rich 2000). For each day, the hourly clearness index k_t at station 2 has been calculated between 11.30 and 12.30 hours (i.e. for the shortest atmospheric path). Then, the diffuse proportion of solar radiation k_d was computed using the regression equation (17) of Orgill and Hollands (1977) for the hourly diffuse fraction

$$k_d = \begin{cases} 1.000 - 0.249k_t & 0 \le k_t < 0.35 \\ 1.557 - 1.840k_t & 0.35 \le k_t < 0.75 \\ 0.177 & k_t > 0.75 \end{cases} \qquad (17)$$

Then the atmospheric transmittivity τ_z at station 2 (1669 m above sea level) was calculated as

$$\tau_z = k_t(1 - k_d) \qquad (18)$$

and corrected for sea level according to the expression

$$\tau_z = \tau_{sl}^{\exp\left(-0.000118z - 1.638 \times 10^{-9}z^2\right)} \qquad (19)$$

which is used internally by *Solar Analyst* to assess the atmospheric transmittivity at any elevation z.

The other required parameter is the proportion of diffuse radiation defined as the proportion of global radiation flux that is diffuse and, calculated by means of the equation (17).

4.2 *r.sun*

This model provides the direct, diffuse and reflected components of the solar radiation. In order to calculate the reflected component the albedo coefficient is required. A constant value of 0.15 has been selected to represent the bare fields and coniferous forest present in the region.

The effect of aerosols (through their total optical depth), of reducing the transmission of direct solar radiation to the surface, is measured by the turbidity. *r.sun* uses the Linke turbidity (T_L) which is defined as the ratio of total optical depth to the Rayleigh optical depth. Figure 2 shows the values of T_L used for each month.

The turbidity coefficient of Linke is a climatologic parameter that characterizes the atmosphere under clear conditions. Therefore, in order to consider the attenuation caused by the clouds, an empirical approach has been used to tune the clear-sky estimates. The ratio K_c of daily global irradiation measured at station 2 to the value for clear-sky conditions estimated with *r.sun* has been used to correct the initial estimates. Then, the actual daily global irradiation G_h can be obtained as

$$G_h = K_c G_{hc} \qquad (20)$$

where K_c is the clear-sky index and G_{hc} is the daily global irradiation simulated for clear-sky conditions.

The representativeness of the clear-sky index at station 2 for the whole study area was tested by comparing the daily measured irradiance series for cloudy days at stations 2, 10 and 14 (which are placed at different elevation levels). A slight delay between irradiance on some stations was observed for some days, but overall, a high level of agreement was detected. Therefore, station 2 can be used to represent the cloudiness on the study area.
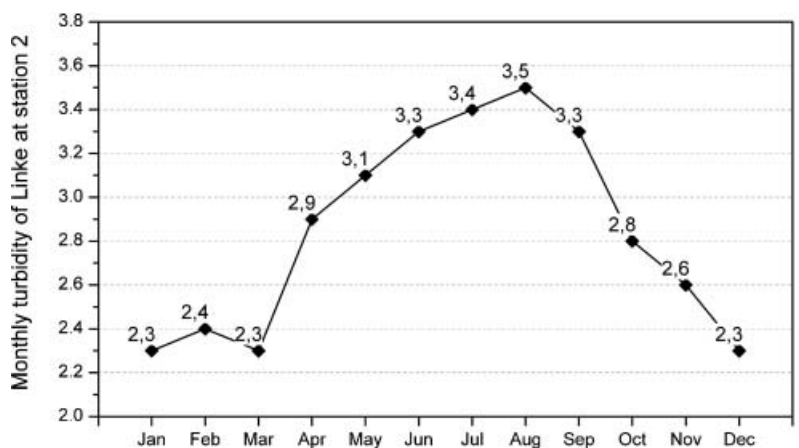
Figure 2. Monthly averages of the turbidity coefficient of Linke from SODA services (http://www.soda-is.com) at the control station 2 (37.147°N, 2.975°W).

4.3 *SRAD*

This model requires a parameter file and optionally, a file specifying vegetation type at every grid cell. The parameter file is made up of 15 lines with information about local monthly properties of atmosphere, temperature, land surface and vegetation. As we are interested just in short-wave radiation, only five parameters have to be locally determined, namely, sunshine fraction, cloudiness parameter, atmospheric transmittivity, circumsolar coefficient and albedo.

Sunshine fraction S is defined as actual number of bright sunshine hours over potential number. The monthly average values for the station 2 have been used (Table 2).

Cloudiness parameter ξ (Table 2) represents the ratio of actual radiation to clear-sky radiation during cloudy periods on an average monthly basis (Wilson and Gallant, 2000). This parameter is seldom available, but can be estimated based on the expression

$$Q_S = Q_0[SF + \xi(1-SF)] \tag{21}$$

where *SF* is the monthly average sunshine fraction, Q_S is the actual monthly average irradiation and Q_0 the monthly average clear-sky irradiation.

Data of cloudiness parameter in Table 2 can be misinterpreted because its value for June, July or August is even higher than for October, November or December. But it should be taken into account that the cloudiness parameter estimates how much attenuation produces an average cloud for a given month rather than the fraction of cloudy skies along that month, which is the object of the sunshine fraction parameter. In fact, equation (21) shows that the higher the sunshine fraction, the smaller the influence of the cloudiness parameter. Note that the factor in brackets in equation (21) reaches its highest value in summer, as it would be expected.

In order to assess Q_0 and Q_S (equation (21)), the daily global irradiation at station 2 has been calculated for each day from March 2003 to January 2006. The actual monthly average irradiation Q_S has been calculated averaging these daily irradiations for each month. To perform the calculation of Q_0, those days with a

Table 2. Monthly average sunshine fraction, cloudiness parameter and atmospheric transmittance used in *SRAD* parameter file.

	Jan	Feb	Mar	Apr	May	Jun	Jul	Aug	Sep	Oct	Nov	Dec
Sunshine fraction	0.57	0.59	0.57	0.63	0.69	0.75	0.80	0.78	0.70	0.62	0.57	0.56
Cloudiness parameter	0.59	0.69	0.22	0.49	0.09	0.56	0.68	0.53	0.28	0.40	0.42	0.44
Atm. transmittance	0.46	0.42	0.34	0.47	0.39	0.51	0.53	0.50	0.45	0.43	0.41	0.42

daily clearness index larger than or equal to 0.7 have been selected and used to assess the monthly average irradiations.

Atmospheric transmittance (Table 2) at sea level τ_{sl} is the monthly average irradiation at sea level relative to the monthly average extraterrestrial irradiation. It is calculated as

$$\tau_{sl} = \tau_z - 0.00008z \tag{22}$$

where τ_z is the atmospheric transmittance at z meters above sea level that has been calculated as Q_S/Q_0.

The circumsolar coefficient represents the proportion of monthly diffuse radiation originated $5°$ within the solar beam direction and should be considered as direct solar radiation. Typical values have been chosen ranging from 0.07 on January to 0.23 on July.

As the case of *r.sun*, the albedo coefficient has been fixed to 0.15, the typical value for bare ground or coniferous forest.

4.4 *Solei-32*

This model, as *r.sun*, only requires the Linke turbidity coefficient (Figure 2), which accounts for the water vapor and aerosols in the atmosphere, integrated all over the spectrum (Louche *et al.* 1986). The results of the simulation are daily solar irradiation, insolation duration and sunrise time.

5. Results

In order to evaluate the role of the DEM's resolution, the solar radiation estimates were obtained with the four radiation models using both the DEM20 and DEM100. An approximated estimation of the execution time spent by the solar models using a HP xw4300 WorkStation with a Pentium® 4 CPU 3.6 GHz and 2 GB of RAM yields the following results: the geometry-based method implemented by *Solar Analyst* is the slowest, with 1500 and 50 seconds for the DEM20 and DEM100, respectively. *r.sun* is the fastest with the DEM100 (4 seconds) but its execution time increases up to 230 seconds with the DEM20. *SRAD* is the fastest with the DEM20 (100 seconds) and only needs 10 seconds to provide the result with the DEM100. *Solei-32* spends 12 seconds with the DEM100 and 375 seconds with the DEM20. Therefore, at these spatial scales, *r.sun* proved to be the most sensitive to the spatial resolution of the DEM whereas *SRAD* was the less affected.

As can be observed in Figure 3(a), (b), (c) and (g), corresponding to 19 September 2005 and characterized by really clear-sky conditions ($k_t = 0.7$), the four models seem to capture the incoming solar variability caused by the considerable topographic
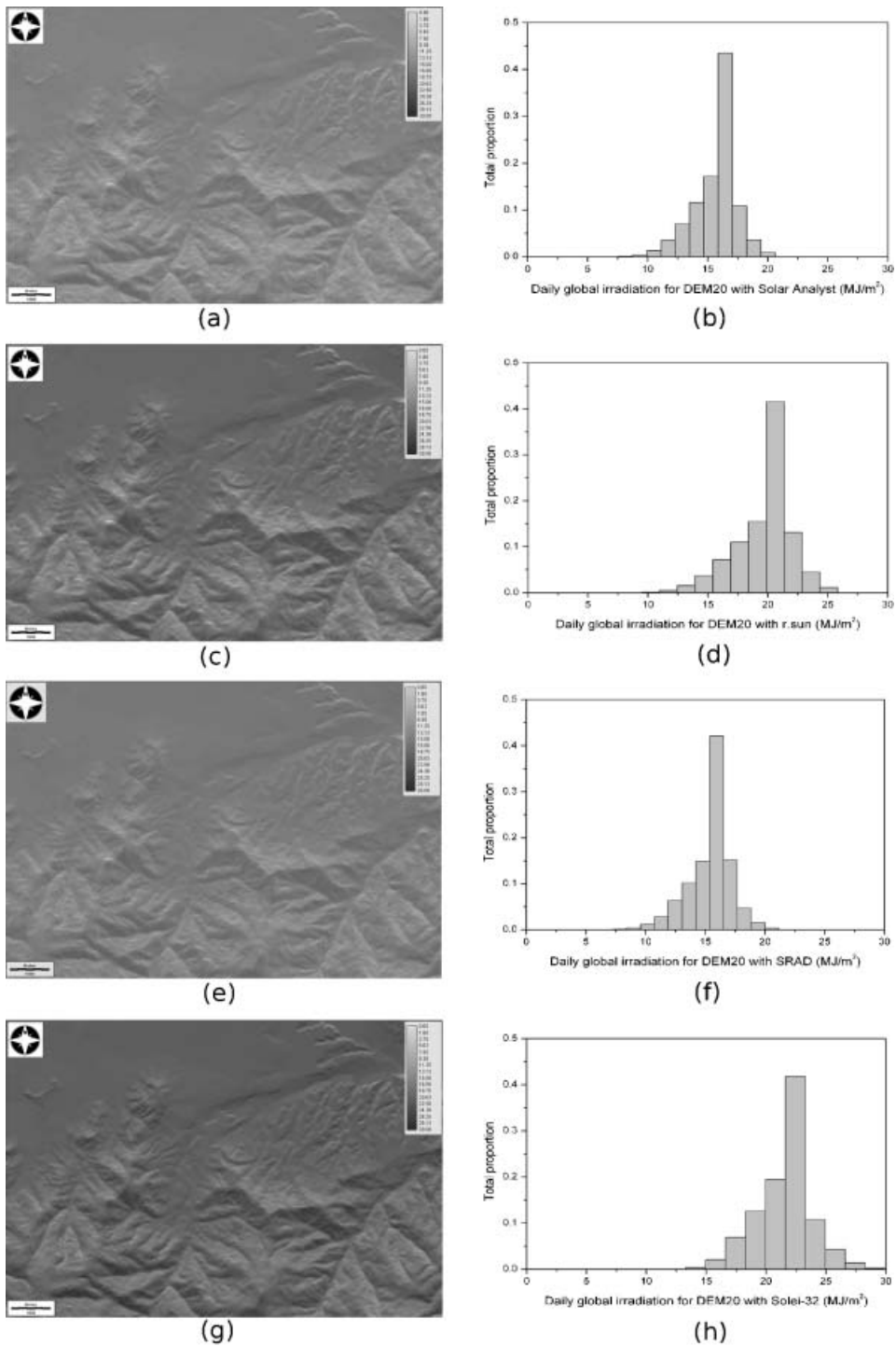
Figure 3. Daily global irradiation (MJ m^{-2}) obtained for 19 September with *Solar Analyst* (a), *r.sun* (c), *SRAD* (e) and *Solei-32* (g) for the study area and the corresponding histograms. The same scale is used for the different maps and histograms.

variability. The histograms corresponding to the solar maps in Figure 3(b), (d), (f) and (h) show a similar shape, which might be derived from the typical distribution of the topographic variables in the study area. Nevertheless, *r.sun* and *Solei-32* provide greater estimates than *Solar Analyst* and *SRAD*, with a mean shift of 4.73 MJ m^{-2}, or 26.70% relative to the mean solar radiation estimate of the four solar radiation models.

We carried out an analysis in order to study the statistical significance of the differences between the different model estimates distributions. To this end, the Kolmogorov–Smirnov statistical test has been used. The analysis was carried out for both the DEM20 and DEM100. Results showed that all the model distributions are statistically different from each other at the 95% significance level, except for the case of the differences between the *r.sun* and the *Solei-32* estimates distributions. Particularly, the *p* values resulting for the tests were 0.5154 for the DEM20 and 0.1452 for the DEM100, proving these two model estimates distributions to be very similar. This fact might be related to the atmospheric modelization used by these solar models, since *r.sun* and *Solei-32* use the turbidity coefficient of Linke for clear-sky conditions, whereas *Solar Analyst* and *SRAD* base their estimates on the atmospheric transmittance.

5.1 *Estimates evaluation*

For each model and DEM, the estimated daily solar radiation data were compared against the data collected in the 14 radiometric-stations. The whole set of experimental data consists of 523 records for each radiation model and spatial resolution (some records were discarded because of the lack of data for all the day or misbehaviors in the sensor's operation). Figure 4 shows the estimated values against the observed one, for each solar model and DEM resolution, and Table 3 presents the corresponding results of the model's evaluation.

To help in the analysis, results of the models evaluation were also obtained depending on the sky conditions. Particularly, sky conditions have been divided based on the clearness-index and the models evaluation was evaluated for days with a clearness-index less than 0.3 (cloudy days), between 0.3 and 0.6 (patchy clouds) and greater than 0.6 (clear sky).

Based on Figure 4(a)–(d) and (g)–(h), it can be concluded that both *Solar Analyst* and, to a lower extent, *r.sun* and *Solei-32*, underestimate the daily global irradiation. *Solar Analyst* estimates have a MBE over four times larger (Table 3) than *r.sun* estimates, regardless of the resolution of the DEM. In the case of *SRAD* (Figure 4(e)–(f)), the estimated values tend to be greater than the observed ones (Table 3). The scattering of the data is especially high for *SRAD*, with a RMSE of 47.64% using the DEM20 and 46.87% using the DEM100.

It can be also observed in Figure 4 that for *Solar Analyst*, *r.sun* and *Solei-32*, those days with the smallest daily global irradiation present a slightly smaller scattering. The rationale behind these results could be that for these days, almost all the solar radiation is diffuse, which is less sensitive to the surrounding topography than the direct radiation.

In general, Table 3 shows very similar results with both resolutions 20 and 100 m, with discrepancies less than 5% in the MBE for all sky conditions. *Solar Analyst* yields a better performance with the DEM20, whereas *r.sun*, *SRAD* and *Solei-32* show better results using the DEM100. Regarding the RMSE, there are no significant differences.
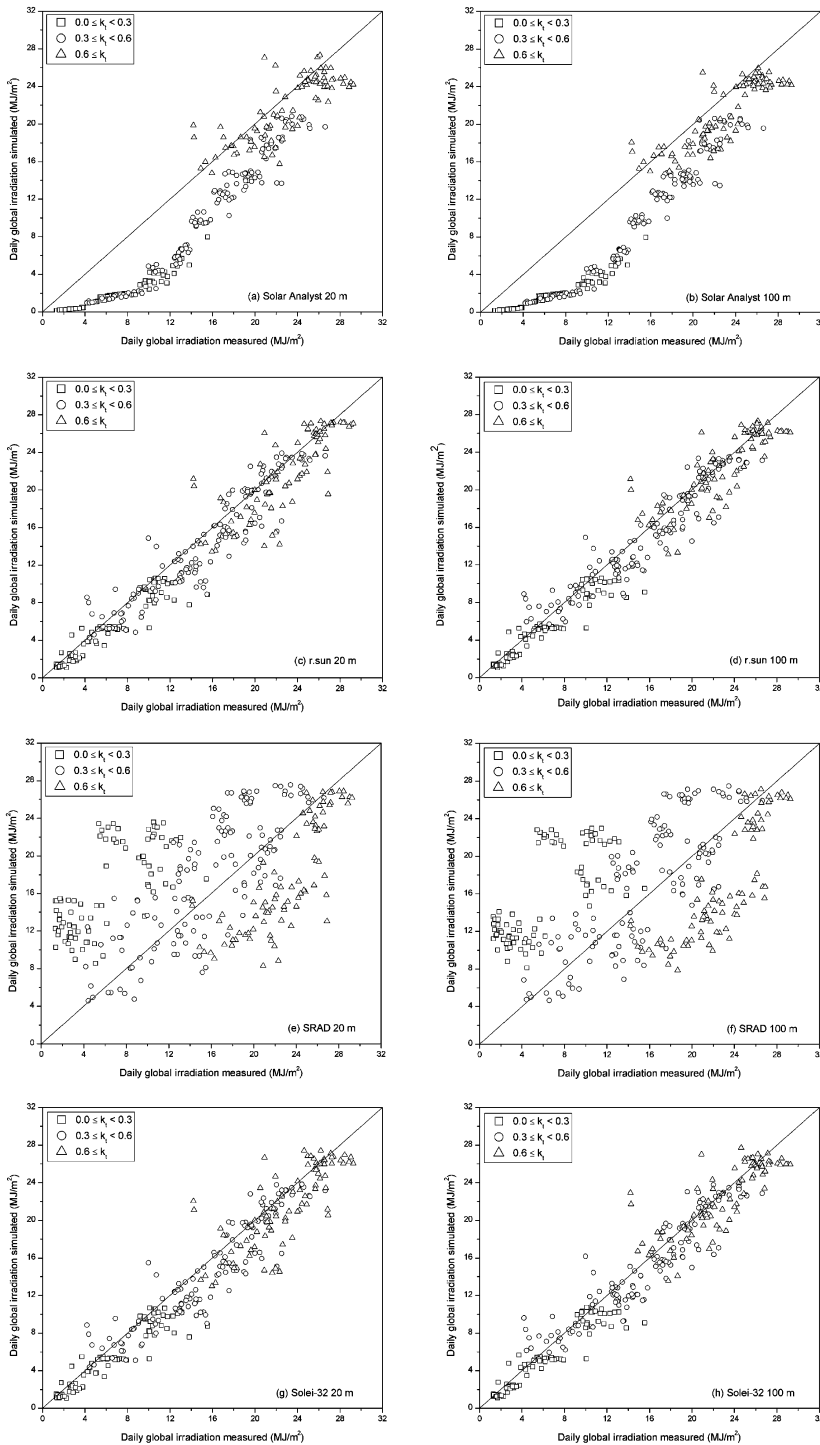
Figure 4.   Daily global irradiation model estimates on inclined surface with the DEM20 and the DEM100 against daily global irradiation measured on inclined surface using *Solar Analyst* (a and b), *r.sun* (c and d), *SRAD* (e and f) and *Solei-32* (g and h). Only a half of the data, representing all sky conditions, are plotted for the sake of clearness.

Table 3. Analysis of the linear relationship between estimated and measured values of daily global irradiation on inclined surfaces. The MBE and RMSE in % are relatives to the mean observed value.

		MBE		RMSE				
		$(MJ\,m^{-2})$	$(\%)$	$(MJ\,m^{-2})$	$(\%)$	Slope	Intercept	r^2
All dataset ($n=523$)								
20 m	Solar Analyst	−3.93	−25.71	4.75	31.10	0.86	5.57	0.91
	r.sun	−1.06	−6.93	2.32	15.26	0.96	1.64	0.93
	SRAD	2.03	13.29	7.28	47.64	0.66	3.82	0.25
	Solei-32	−1.17	−7.68	2.45	16.05	0.97	1.62	0.92
100 m	Solar Analyst	−.07	−26.60	4.77	31.19	0.88	5.46	0.92
	r.sun	−0.70	−4.61	1.99	13.09	0.98	1.05	0.94
	SRAD	1.51	9.86	7.16	46.87	0.65	4.40	0.26
	Solei-32	−0.66	−4.32	2.05	13.46	0.97	1.04	0.94
$k_t \leqslant 0.3$ ($n=132$)								
20 m	Solar Analyst	−4.51	−70.63	5.05	78.98	2.19	2.29	0.93
	r.sun	−1.05	−16.39	1.73	27.12	1.11	0.47	0.88
	SRAD	10.06	157.50	10.67	166.95	0.56	−2.75	0.44
	Solei-32	−1.09	−17.01	1.80	28.15	1.11	0.50	0.87
100 m	Solar Analyst	−4.49	−70.31	5.02	78.63	2.18	2.25	0.94
	r.sun	−0.90	−14.08	1.61	25.20	1.11	0.31	0.89
	SRAD	9.48	148.42	10.12	158.37	0.55	−2.38	0.48
	Solei-32	−0.89	−13.93	1.63	25.49	1.10	0.33	0.88
$0.3<k_t \leqslant 0.6$ ($n=252$)								
20 m	Solar Analyst	−5.12	−32.65	5.34	34.05	0.86	6.56	0.94
	r.sun	−1.02	−6.51	2.31	14.69	0.90	2.44	0.86
	SRAD	2.03	12.96	4.52	28.82	0.65	4.26	0.63
	Solei-32	−1.12	−7.15	2.40	15.30	0.92	2.36	0.85
100 m	Solar Analyst	−5.14	−32.76	5.37	34.22	0.86	6.60	0.94
	r.sun	−0.69	−4.42	2.03	12.96	0.98	0.99	0.88
	SRAD	1.55	9.85	4.38	27.91	0.63	4.82	0.64
	Solei-32	−0.64	−4.05	2.06	13.11	0.98	0.92	0.89
$0.6<k_t$ ($n=139$)								
20 m	Solar Analyst	−1.27	−5.54	2.64	11.51	0.89	3.66	0.64
	r.sun	−1.13	−4.94	2.80	12.22	0.71	7.54	0.65
	SRAD	−5.44	−23.77	6.51	28.41	0.52	13.81	0.63
	Solei-32	−1.33	−5.79	2.99	13.04	0.70	7.90	0.61
100 m	Solar Analyst	−1.75	−7.61	2.63	11.46	0.93	3.16	0.73
	r.sun	−0.54	−2.35	2.25	9.80	0.85	3.93	0.69
	SRAD	−5.97	−26.04	6.98	30.45	0.52	14.17	0.68
	Solei-32	−0.47	−2.06	2.38	10.37	0.84	4.12	0.64

We carried out an analysis in order to study the statistical significance of the differences between the models estimates at the 14 station locations and these station measurements. Again, the Kolmogorov–Smirnov statistical test has been used. Results showed that differences between *Solar Analyst* and *SRAD* estimates distributions and the ground data distributions were statistically significant at the 99% confidence level. This result holds both for the DEM20 and the DEM100. For the case of *r.sun* and *Solei-32*, differences between model estimates distributions and ground data distributions were shown not to be statistically significant, both for the

DEM100 case ($p=0.29$ for *r.sun* and *Solei-32*) and the DEM20 case ($p=0.15$ for *r.sun* and 0.12 for *Solei-32*).

An additional analysis, using the *t*-test, was carried out to test for differences between model estimates means and ground measured data means. Results proved to be similar to those obtained using the Kolmogorov–Smirnov significance test. Particularly, the differences between *Solar Analyst* and *SRAD* model estimates mean values and ground data mean values proved to be statistically significant at the 99% level (both using the DEM20 and the DEM100). For the case of *Solei-32*, result differences are statistically significant at the 95% when using the DEM20, and not statistically significant when using the DEM100 ($p=0.29$). Finally, for the *r.sun* case, the test clearly shows that result differences are statistically significant at the 95% using the DEM20, and not statistically significant using the DEM100 ($p=0.26$).

To sum up, the different test results showed that *r.sun* and *Solei-32* are able to reasonably reproduce the ground data distribution, regardless of the spatial resolution of the DEM. However, both *Solar Analyst* and *SRAD* are not able to reproduce the ground data distribution.

5.1.1 Solar Analyst evaluation. *Solar Analyst* generally underestimates the observed daily irradiation, especially for those days with a clearness-index below 0.3. When the clearness-index is between 0.3 and 0.6, underestimating error slightly decreases, as the daily irradiation increases. In the case of days with a clearness-index greater than 0.6, the scattering of the data increases and some days even show estimated values above the observed ones. Note that, under overcast conditions ($k_t<0.3$), the underestimation seems to indicate a lower reliability of the solar diffuse radiation model. On the other hand, for partly cloudy days, the clouds may cause a high intra-hourly variability on the solar radiation that, if it occurs around noon (between 11:30 and 12:30), it can introduce some noise in the calculated direct transmittance of the atmosphere for that day. This problem is not present under completely overcast or clear days, where the atmospheric attenuation by clouds may be considered homogeneous.

5.1.2 r.sun evaluation. This model provides the estimation based on the turbidity coefficient of Linke for clear-sky conditions. Then, the irradiation in the whole area has been modified according to the observed value at the station 2. This adjustment is very important in cloudy days and almost negligible in clear days. The model estimates show a reasonable agreement with the observed data, with just a small underestimation and a relatively low scattering. The MBE remains approximately the same regardless of the sky conditions, but its relative value decreases from -16.39% (-14.08%) under overcast conditions to -4.94% (-2.35%) under clear skies with the DEM20 (DEM100). The relative RMSE also decreases from 27.12% (25.20%) to 12.22% (9.80%) when sky conditions become clearer using the DEM20 (DEM100). These results show a slightly better performance of the model with the DEM100.

5.1.3 SRAD evaluation. This model uses monthly averaged parameters to modify an initial estimation. Figure 4(e)–(f) shows a large scattering on the estimates, probably influenced by the short length of the climatologic record used to estimate these parameters. *SRAD* overestimates the observed values and presents the largest MBE and RMSE (even greater than 100%) for days with a clearness-index less than 0.3, probably because of the small value of the solar radiation under overcast conditions. The estimated values improve for days with a clearness-index between

0.3 and 0.6: relative MBE over 13% and relative RMSE over 29% with the DEM20. The relative MBE of the estimates values improves over 3% using the DEM100. For days with a clearness-index above 0.6, the model underestimates the observed values with a relative MBE over −25% and a relative RMSE over 30%. Therefore, *SRAD* shows a noticeable overestimation under overcast skies and a fair underestimation under clear conditions. Better results have been reported by Reuter *et al.* (2005) in Luettewitz (Germany), a study area with a less topographic complexity, using a method to correct the estimates with measurements at the reference site.

5.1.4   Solei-32 evaluation. This model yields solar radiation estimates based on the turbidity coefficient of Linke. Therefore, as has been already commented for the case of *r.sun*, it needs a subsequent adjustment to account for the cloud attenuation. For a clearness-index smaller than 0.3, *Solei-32* underestimates the observed values with a relative MBE of −17.01% using the DEM20 and −13.93% using the DEM100. The relative RMSE is over 25% with the two DEMs. For partly cloudy days, the performance improves up to a relative MBE of −1.12% using the DEM20 and −0.64% using the DEM100. The relative RMSE decreases up to around 13–15%. For completely clear conditions, the model overestimates the observed values with a relative MBE of −1.33 and −0.47% for the DEM20 and the DEM100, respectively, while the relative RMSE decreases up to 13% with the DEM20 and up to 10.37% with the DEM100.

5.2   *Sensitivity to the resolution of the DEM*

Aiming to study the sensitivity of the different solar radiation models to the DEM resolution, simulated values resulting from DEM100 and DEM20 have been compared with each other. This analysis was carried out separately for the different sky conditions, allowing evaluating, separately, the diffuse and the direct radiation models implemented within each solar radiation model. Figure 5 shows the results for the whole dataset while Table 4 presents the statistic of the analysis.

When analyzing the whole sky conditions (Table 4), *Solar Analyst* presents the lowest RMSD, with a value around 5.78%. The remaining solar radiation models present values around 9%. This result keeps when analyzing separately the different sky conditions, in all the cases, the *Solar Analyst* yields the lowest RMSD values. It could then be concluded that *Solar Analyst* presents the lowest sensitivity to the DEM resolution. The rationale behind these results could be that the diffuse model of the *Solar Analyst* is especially independent of the topography. Note (Table 4) that the RMSD value for completely overcast days (all the radiation is practically diffuse) is lower (2.96%) than the value for completely clear days (all the radiation is practically direct) (5.39%). The rest of the models do not present this differenced behavior, with very similar RMSD values for all the sky conditions.

Another way to evaluate the sensitivity of the model estimates to the topography is by analyzing separately the model estimates for each location of the ground stations. Figure 6 shows the RMSE of the daily irradiation estimates separately at each station location. The analysis is carried out for each of the four solar radiation models using the DEM100 (very similar results are found when using the DEM20) and as a function of the sky conditions.

Particularly, from Figure 6, it can be concluded that *r.sun* and *Solei-32* estimates are very similar and yield the lowest RMSE values, regardless of the sky conditions.
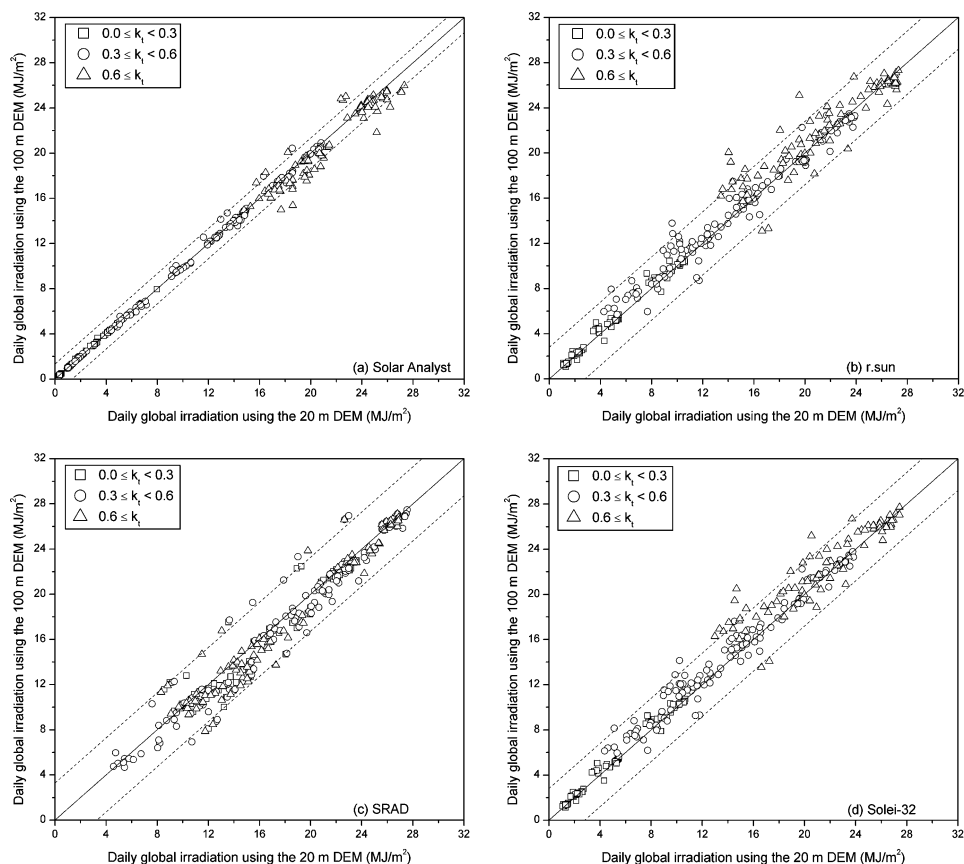
Figure 5. Daily global irradiation on inclined surface (for the 14 radiometric station locations) simulated with the DEM100 against simulated with DEM20 using *Solar Analyst* (a), *r.sun* (b), *SRAD* (c) and *Solei-32* (d). The dashed lines represent the region that contains the 95% of the data. Only a half of the data, representing all sky conditions, are plotted for the sake of clearness.

Note that for these two solar radiation models, the RMSE in station 2 is identically zero because it was selected as a control station to adjust the preliminary estimates according to the actual cloud attenuation process.

For overcast conditions, the solar models present a small variability in the RMSE values between stations, probably because most of the radiation is of diffuse nature. Particularly, the variability of the RMSE in *Solar Analyst* between the stations is especially small, consistent with the results in Table 4.

On the other hand, the variability increases for all the solar models under patchy clouds and clear-days conditions, since the direct component of the solar radiation becomes more important than the diffuse component. For partly overcast skies, the RMSE values of *SRAD* become even smaller than those of the *Solar Analyst.* This is probably related to the difficult estimation of the input parameters for these sky conditions in *Solar Analyst*. However, under completely clear days, the *Solar Analyst* RMSE values decrease up to almost the level of *r.sun* and *Solei-32* and the *SRAD* RMSE values become even greater than for patchy conditions. This late result is explained by the fact that *SRAD* bases their estimates on monthly averaged

Table 4. Analysis of the linear relationship between estimated daily global irradiation on inclined surface using 20 m resolution and 100 m resolution DEMs for the 14 radiometric station locations. The MBD and RMSD are defined as in equations (15) and (16) but using the two series of estimates with the DEM20 and DEM100 rather than an estimated series and a measured series. The values in % are relatives to the mean of the two estimated series.

| | MBD | | RMSD | | | | |
	$(MJ\,m^{-2})$	(%)	$(MJ\,m^{-2})$	(%)	Slope	Intercept	r^2
All dataset ($n=523$)							
Solar Analyst	0.14	1.20	0.65	5.78	1.02	−0.04	0.99
r.sun	−0.38	−2.51	1.35	8.97	0.99	−0.22	0.98
SRAD	0.52	3.07	1.56	9.13	0.93	1.62	0.94
Solei-32	−0.51	−3.51	1.26	8.63	0.99	0.66	0.98
$k_t \leqslant 0.3$ ($n=132$)							
Solar Analyst	−0.02	−1.10	0.06	2.96	0.99	−0.01	0.99
r.sun	−0.15	−2.73	0.42	7.82	0.98	−0.08	0.98
SRAD	0.58	3.59	1.56	9.68	0.91	1.96	0.91
Solei-32	−0.20	−3.58	0.43	7.78	1.01	0.15	0.99
$0.3 < k_t \leqslant 0.6$ ($n=252$)							
Solar Analyst	0.02	0.16	0.34	3.17	0.99	0.04	0.99
r.sun	−0.33	−2.21	1.14	7.67	1.06	−1.19	0.96
SRAD	0.49	2.79	1.53	8.75	0.95	1.42	0.96
Solei-32	−0.49	−3.23	1.12	7.42	0.93	1.57	0.97
$0.6 < k_t$ ($n=139$)							
Solar Analyst	0.48	2.22	1.15	5.39	0.93	1.96	0.91
r.sun	−0.60	−2.72	1.86	8.41	1.07	−2.25	0.84
SRAD	0.53	3.08	1.59	9.25	0.93	1.80	0.94
Solei-32	−0.85	−3.81	1.86	8.27	0.79	5.47	0.86

parameters and the reliability decreases for days with extreme conditions. Note that all these results are consistent with the statistics shown in Table 3.

Based on the topographic conditions of the station locations, presented in Figure 1 and Table 1, some conclusion can be derived from the former analysis. The stations have been grouped in two sets according to its topographic complexity based on the surface slope. Stations 5, 7 and 12–14 have been included in a first group, with low topographic complexity, and stations 3, 6, 8, 9 and 11 have been included in a second group of high topographic complexity. The comparison of the RMSE values of these two groups of stations did not yield significant conclusions for overcast and partly overcast skies. However, for clear days and all the solar models, overall, lower RMSE values (between 1 and 2.5%) were observed for the low topographic complexity stations than for the high topographic complexity stations. Additionally, when using the DEM20 (figure not shown), the RMSE decreased more than 5% in *r.sun* and *Solei-32*, 4% in *Solar Analyst* and 3% in *SRAD*.

It can then be concluded that only under clear-sky conditions may the topography of the study area play an important role for the solar models estimates reliability. Particularly, under these sky conditions, differences of up to 3% in RMSE can be found when comparing very complex topography locations and low complex topography locations. Consequently, for clear conditions, based on the former
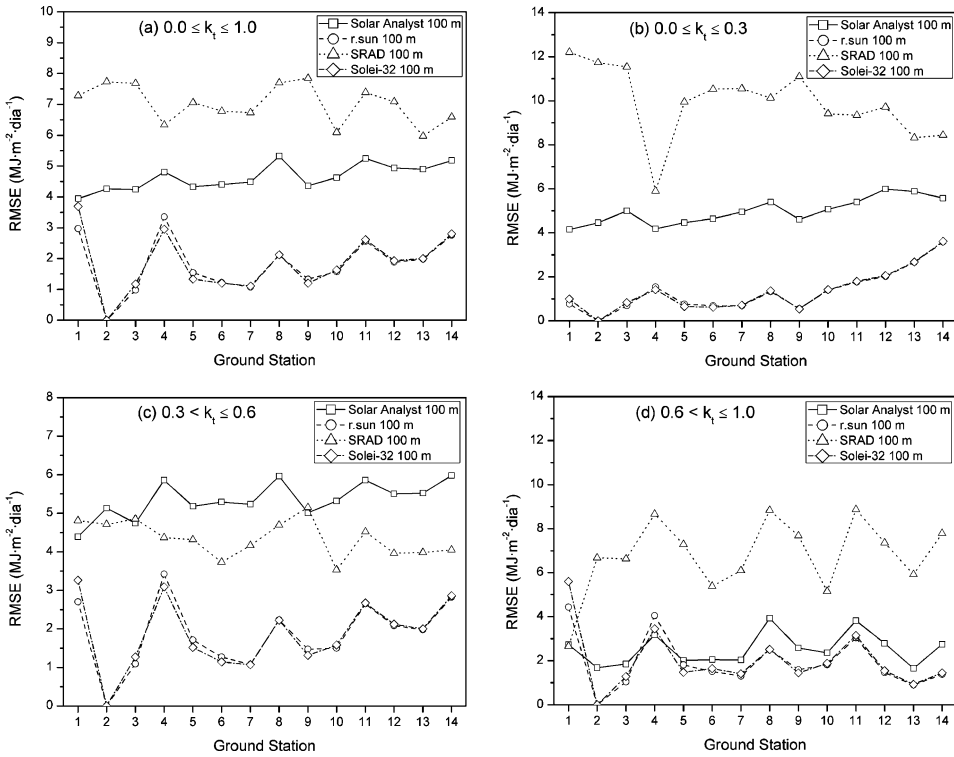
Figure 6. RMSE (MJ m^{-2}) of the daily solar radiation models estimates for every ground station using the DEM100: (a) for the whole dataset, (b) for overcast conditions, (c) for patchy clouds days and (d) for clear sky conditions.

analysis, an improvement is expectable in the solar models estimates for complex topography areas by increasing the resolution of the DEM. Nevertheless, this improvement may not be achieved under more general sky conditions, because the errors in the diffuse component (which is just slightly dependent of the topography) might mask this improvement.

In order to assess the role of the DEM resolution to determine the influence of the shadow castings on the solar radiation model estimates, an additional analysis was carried out. Particularly, two clear-sky days with different solar height were selected: 18 February 2005, with a solar height of 40.84° and a clearness-index of 0.75, and 14 August 2005, with a solar height of 67.36° and a clearness-index of 0.68. Model estimates using both the DEM20 and the DEM100 were compared against observations for the two days. Table 5 shows the results. The topography obviously causes stronger shadow casting on 18 February because of the smaller solar height. Overall, smaller RMSE and MBE (in module) are observed for 14 August using both the DEM20 and the DEM100. Moreover, for 18 February, the DEM20 provides slightly better estimates than the DEM100, while for 14 August, errors are very similar with both resolutions. The results of this analysis suggest that when large shadow-casting are presented, an increment of the DEM resolution provides better global radiation estimates. Nevertheless, this conclusion should be cautiously considered given the relatively small analysed record (only 14 records per day).

Table 5. Analysis of the linear relationship between estimated and measured values of daily irradiation on inclined surface for 18 February 2005 and 14 August 2005. Models estimates results for both the DEM20 and the DEM100 are displayed.

		MBE		RMSE				
		$(MJ\,m^{-2})$	(%)	$(MJ\,m^{-2})$	(%)	Slope	Intercept	r^2
18 February 2005 ($n=14$) Daily clearness-index: 0.75 Solar height: 40.84°								
20 m	Solar Analyst	−0.49	−2.57	2.68	14.21	0.49	9.78	0.08
	r.sun	−1.60	−8.46	3.74	19.83	0.18	15.81	0.03
	SRAD	−7.29	−38.61	7.94	42.07	0.11	17.60	0.01
	Solei-32	−1.65	−8.76	3.94	20.85	0.10	17.20	0.01
100 m	Solar Analyst	−1.39	−7.34	2.72	14.39	1.15	−1.18	0.22
	r.sun	−0.21	−1.12	2.97	15.72	0.33	12.81	0.08
	SRAD	−8.26	−43.77	8.69	46.03	0.41	14.50	0.04
	Solei-32	−0.05	−0.31	3.20	16.94	0.13	16.48	0.01
14 August 2005 ($n=14$) Daily clearness-index: 0.68 Solar height: 67.36°								
20 m	Solar Analyst	−0.89	−3.47	1.33	5.17	0.27	19.08	0.09
	r.sun	0.41	1.57	1.16	4.51	0.19	20.72	0.05
	SRAD	−2.17	−8.42	2.58	10.04	0.16	21.88	0.09
	Solei-32	−0.01	−0.03	1.30	5.05	0.10	23.21	0.02
100 m	Solar Analyst	−1.08	−4.19	1.33	5.17	0.52	12.85	0.13
	r.sun	0.48	1.87	1.06	4.12	0.26	19.03	0.06
	SRAD	−2.40	−9.31	2.55	9.93	0.36	17.34	0.12
	Solei-32	0.53	2.07	1.16	4.51	0.08	23.60	0.01

5.3 *Seasonal reliability of the solar radiation models*

In order to evaluate the relative performance of the solar radiation models along the year, we have compared the MBE and RMSE of the four models estimates for each season of the year. Figure 7 shows the results of this analysis, using the DEM100 model (similar results are obtained when using the DEM20). Figure 7(a) presents the MBE analysis results, with an overall underestimation for all the models except
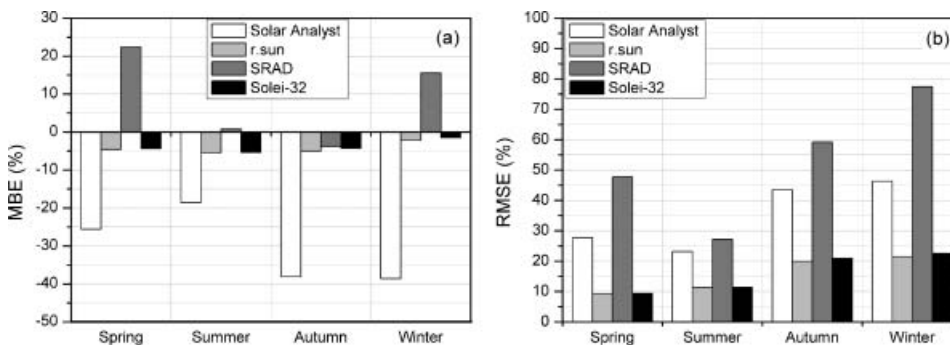

Figure 7. MBE (a) and RMSE (b) for the solar radiation models using the DEM100 for each season of the year.

SRAD. *Solar Analyst* presents the greatest MBE values, ranging from around -20% in summer to almost -40% in autumn and winter. *SRAD* overestimates the measured values on spring and winter and it underestimates them on autumn. Interestingly, the mean error is practically negligible on summer. On the other hand, *r.sun* and *Solei-32* have a mean error below 10% along the whole year.

Concerning the RMSE analysis results (Figure 7(b)), again the best results are found for spring and summer for all the solar radiation models. Particularly, results provided by *r.sun* and *Solei-32* show the lowest RMSE values: around 10% during spring and summer and around 20% in autumn and winter. *Solar Analyst* shows values ranging from 25% in summer to 45% in autumn. Finally, *SRAD* RMSE values range over 25% on summer up to 75% on winter.

6. Conclusions

In this work, the reliability of the daily global radiation estimates in complex topography areas of four up-to-date spatially-distributed solar radiation models (*Solar Analyst*, *r.sun*, *SRAD* and *Solei-32*) has been evaluated. In order to study the role of the spatial resolution of the DEM on these solar radiation estimates, the analysis was carried out using two different resolutions: 20 and 100 m. The estimates were tested using a database provided by 14 radiometric stations located in the National Park of Sierra Nevada (south-eastern Spain), with horizontal and inclined measurements of global solar radiation.

Overall, results showed that the solar radiation variability can be reasonably estimated under clear-sky conditions using these DEM-based models (*r.sun* and *Solei-32* reported a MBE of around -4.5% and a RMSE of around 13% for all the studied dataset, using a DEM with 100 m of spatial resolution). Under cloudy skies, the reliability decreases because of the uncertainties in parameterization of atmospheric conditions and processes. For this reason, all these models need, at some stage of the estimation process, to use experimental data in order to accommodate the estimates to the actual values. To this end, two approaches can be followed: either to use the observed data to parameterize the state of the atmosphere before the estimate is provided (as is the case of *Solar Analyst* and *SRAD*), or to use the observed data to correct the estimate (as is the case of *r.sun* and *Solei-32*). The result of this work suggests that better estimates can be achieved when the second approach is followed.

Particularly, the *Solar Analyst* model needs the direct atmospheric transmittivity along the shortest atmospheric path. This parameter is really sensitive to the presence of clouds (see Section 5.1), making difficult to provide a correct value. In the case of *SRAD*, their estimates are adjusted by means of monthly averages of certain parameters as sunshine fraction, cloudiness or atmospheric transmittance. As a consequence, the longer the climatology, the better the estimations. In practice, it is difficult to dispose of a long enough climatology, this being the main pitfall of this model. On the other side, the use of monthly average parameters makes *SRAD* suitable for applications such as biologic or geologic studies. Additionally, it presents the advantage of providing the complete radiation budget, and not only the short-wave radiation.

On the other side, *r.sun* and *Solei-32* use a different approach to model the atmospheric attenuation. These two models compute the solar radiance for clear-sky conditions based on the turbidity coefficient of Linke, which can be obtained for a specific latitude, day and height, or even queried on a database. Then, they use

ground stations measurements to tune the initial estimate. The main weakness of this approach is to find a station representative of the whole study area. This is particularly difficult in complex topography areas. Nevertheless, to overcome this problem, more than one station could be used to carry out a spatial interpolation analysis, and then to obtain a surface for the study area representing the spatially-distributed cloud attenuation (Súri *et al.* 2004).

We analyzed the sensitivity of the model estimates to the DEM resolution and to the topographic characteristics of the study area. Results showed that under clear-sky conditions (or strong shadow-castings), the topography of the study area may play an important role for the model estimates reliability. Under these circumstances, an improvement is expectable in the model estimates by increasing the resolution of the DEM, and the use of a higher spatial resolution (as the DEM20, in our case) should be considered. Nevertheless, this improvement may not be present under more general sky conditions, because the errors in the diffuse component (which is just slightly dependent of the topography) might mask this improvement.

Throughout the year, the reliability of the *Solar Analyst* and *SRAD* estimates decreases in autumn and winter, whereas the performance of *r.sun* and *Solei-32* remain quite constant. Therefore, the best results are provided by *r.sun* and *Solei-32*. The rationale behind this can be that the increase in the atmospheric complexity during autumn and winter make the parameterization of the atmosphere in *Solar Analyst* and *SRAD* difficult.

Acknowledgements

References

BATLLES, F.J., BOSCH, J.L., TOVAR-PESCADOR, J., MARTÍNEZ-DURBÁN, M., ORTEGA, R. and MIRALLES, I., 2008, Determination of atmospheric parameters to estimate global radiation in areas of complex topography: generation of global irradiation map. *Energy Conversion and Management*, **49**, pp. 336–345.

BEYER, H.G., CZEPLAK, G., TERZENBACH, U. and WALD, L., 1997, Assessment of the method used to construct clearness index maps for the new European solar radiation atlas (ESRA). *Solar Energy*, **61**, pp. 389–397.

CORRIPIO, J.G., 2003, Vectorial algebra algorithms for calculating terrain parameters from DEMs and solar radiation modelling in mountainous terrain. *International Journal of Geographical Information Science*, **17**, pp. 1–23.

DUBAYAH, R. and RICH, P.M., 1995, Topographic solar-radiation models for GIS. *International Journal of Geographical Information Science*, **9**, pp. 495–519.

DUBAYAH, R. and RICH, P.M., 1996, GIS-based solar radiation modelling in GIS. In M.F. Goodchild, L.T. Steyaert, B.O. Parks, C. Johnston, D. Maidment, M. Crane and S. Glendinning (Eds), *Environmental Modelling: Progress and Research Issues*, pp. 129–135 (Fort Collins, CO: GIS World Books).

FLEMING, P.M., 1987, Notes on a radiation index for use in studies of aspect effects on radiation climate (Canberra: Commonwealth Scientific and Industrial Research Organization, Division of Water Resources Research, Institute of Biological Resources Technical Memorandum).

Fu, P. and Rich, P.M., 2000, *The Solar Analyst 1.0. User Manual* (Vermont, KS: Helios Environmental Modeling Institute).

Fu, P. and Rich, P.M., 2002, A geometric solar radiation model with applications in agriculture and forestry. *Computers and Electronics in Agriculture*, **37**, pp. 25–35.

Hetrick, W.A., Rich, P.M., Barnes, F.J. and Weiss, S.B., GIS-based solar radiation flux models. In *GIS Photogrammetry and Modeling*, Vol. 3, pp. 132–143 (Bethesda, MD: American Society for Photogrammetry and Remote Sensing).

Hofierka, J., 1997, Direct solar radiation modelling within an open GIS environment In *Proceedings of the Joint European GIS Conference 1997*, April 1997, Vienna, Austria, pp. 575–584.

Hofierka, J. and Súri, M., 2002, The solar radiation model for open source GIS: implementation and applications. In *Proceedings of the Open Source GIS-GRASS Users Conference*, September 2002, Trento, Italy, pp. 1–19.

Hulme, M., Conway, D., Jones, P.D., Jiang, T., Barrow, E.M. and Turney, C., 1995, A 1961–1990 climatology for Europe for climate change modelling and impact applications. *International Journal of Climatology*, **15**, pp. 1333–1364.

Jeffrey, S.J., Carter, J.O., Moodie, K.B. and Beswick, A.R., 2001, Using spatial interpolation to construct a comprehensive archive of Australian climate data. *Environmental Modelling and Software*, **16**, pp. 309–330.

Kondratyev, K., 1965, *Radiative Heat Exchange in the Atmosphere* (New York: Pergamon Press).

Kumar, L., Skidmore, A.K. and Knowles, E., 1997, Modelling topographic variation in solar radiation in a GIS environment. *International Journal of Geographical Information Science*, **11**, pp. 475–497.

Kumar, L. and Skidmore, A.K., 2000, Radiation–vegetation relationships in a eucalyptus forest. *Photogrammetric Engineering and Remote Sensing*, **2**, pp. 193–204.

Leemans, R. and Wolfgang, P.C., 1991, The IIASA Database for Mean Monthly Values of Temperature, Precipitation and Cloudiness of a Global Terrestrial Grid. Report RR-91-18 (Laxenburg: IIASA).

Lopez, G., Batlles, F.J. and Tovar-Pescador, J., 2007, A new simple parameterization of daily clear-sky global solar radiation including horizon effects. *Energy Conversion and Management*, **48**, pp. 226–233.

Louche, A., Peri, G. and Iqbal, M., 1986, An analysis of Linke turbidity factor. *Solar Energy*, **37**, pp. 393–396.

McKenney, D.W., MacKey, B.G. and Zavitz, B.L., 1999, Calibration and sensitivity analysis of a spatially-distributed solar radiation model. *International Journal of Geographical Information Science*, **13**, pp. 49–65.

McVicar, T.R., Van Niel, T.G., Li, L., Hutchinson, M.F., Mu, X. and Liu, Z., 2007, Spatially distributing monthly reference evapotranspiration and pan evaporation considering topographic influences. *Journal of Hydrology*, **338**, pp. 196–220.

Mészáros, I., Miklánek, P. and Parajka, J., 2002, Solar energy income modelling in mountainous areas. In L. Holko, P. Miklánek, J. Parajka and Z. Kostka (Eds), *ERB and NEFRIEND Proj.5 Conf. Interdisciplinary Approaches in Small Catchment Hydrology: Monitoring and Research*, pp. 127–135 (Bratislava: Slovak NC IHP UNESCO/UH SAV).

Miklánek, P. and Mészáros, I., 1993, Modelling of insolation characteristics in mountainous environment. In *Advances in Water Sciences*, Vol. II, Hydrological processes and transport phenomena in environment, pp. 32–36 (Stara Lesna: UH SAV).

Oliphant, A.J., Spronken-Smith, R.A., Sturman, A.P. and Owens, I.F., 2003, Spatial variability of surface radiation fluxes in mountainous region. *Journal of Applied Meteorology*, **42**, pp. 113–128.

O'Loughlin, E.M., 1990, Modelling soil water status in complex terrain. *Journal of Applied Meteorology*, **50**, pp. 23–38.

ORGILL, J.F. and HOLLANDS, K.G.T., 1977, Correlation equation for hourly diffuse radiation on a horizontal surface. *Solar Energy*, **19**, pp. 357–359.

PAGE, J.K., ALBUISSON, M. and WALD, L., 2001, The European solar radiation atlas: a valuable digital tool. *Solar Energy*, **71**, pp. 81–83.

RAAFLAUB, L.D. and COLLINS, M.J., 2006, The effect of error in gridded digital elevation models on the estimation of topographic parameters. *Environmental Modelling and Software*, **21**, pp. 710–732.

REUTER, H.I., KERSEBAUM, K.C. and WENDROTH, O., 2005, Modelling of solar radiation influenced by topographic shading – evaluation and application for precision farming. *Physics and Chemistry of the Earth*, **30**, pp. 143–149.

SAMPSON, P.D. and GUTTORP, P., 1992, Nonparametric-estimation of non-stationary spatial covariance structure. *Journal of the American Statistical Association*, **87**, pp. 108–119.

SCHEIFINGER, H. and KROMP-KOLB, H., 2000, Modeling global radiation in complex terrain: comparing two statistical approaches. *Agricultural and Forest Meteorology*, **100**, pp. 127–136.

SÚRI, M. and HOFIERKA, J., 2004, A new GIS-based solar radiation model and its application to photovoltaic assessments. *Transactions in GIS*, **2**, pp. 175–190.

SÚRI, M., HULD, T.A. and DUNLOP, E.D., 2005, PV-GIS: a web-based solar radiation database for the calculation of PV in potential in Europe. *International Journal of Sustainable Energy*, **24**, pp. 55–67.

TOVAR, J., OLMO, F.J. and ALADOS-ARBOLEDAS, L., 1995, Local Scale Variability of Solar radiation in a Mountainous Region. *Journal of Applied Meteorology*, **34**, pp. 2316–2322.

TOVAR-PESCADOR, J., POZO-VÁZQUEZ, D., RUIZ-ARIAS, J.A., BATLLES, J., LÓPEZ, G. and BOSCH, J.L., 2006, On the use of the digital elevation model to estimate the solar radiation in areas of complex topography. *Meteorological Applications*, **13**, pp. 279–287.

WILSON, J.P. and GALLANT, J.C., 2000, *Terrain Analysis: Principles and Applications* (New York: John Wiley and Sons).

XIA, Y., WINTERHALTER, M. and FABIAN, P., 2000, Interpolation of daily global solar radiation with thin plate smoothing splines. *Theoretical and Applied Climatology*, **66**, pp. 109–115.

ZELENKA, A., CZEPLAK, G., D'AGOSTINO, V., JOSEFSON, W., MAXWELL, E. and PEREZ, R., 1992, Techniques for supplementing solar radiation network data. Technical Report, International Energy Agency, IEA-SHCP-9D-1, Swiss Meteorological Institute, Switzerland.